Thin Solid Films 739 (2021) 138980

Contents lists available at ScienceDirect

Thin Solid Films

journal homepage: www.elsevier.com/locate/tsf

Characterization of tetrahedrite $Cu_{10}Cd_2Sb_4S_{13}$ monograin materials grown in molten CdI_2 and LiI

Fairouz Ghisani [a,*], Kristi Timmo [a], Mare Altosaar [a], Valdek Mikli [a], Maris Pilvet [a], Reelika Kaupmees [a], Jüri Krustok [a,b], Maarja Grossberg [a], Marit Kauk-Kuusik [a]

[a] Department of Materials and Environmental Technology, Tallinn University of Technology, Ehitajate tee 5, 19086 Tallinn, Estonia
[b] Division of Physics, Tallinn University of Technology, Ehitajate Tee 5, Tallinn 19086, Estonia

ARTICLE INFO

Keywords:
Tetrahedrites
Molten salt synthesis-growth
Absorbers
Photoluminescence
Raman spectroscopy

ABSTRACT

Synthesis of Cd-substituted tetrahedrite $Cu_{10}Cd_2Sb_4S_{13}$ (TH—Cd) monograin powders are performed by the molten salt synthesis-growth method using two different fluxes: CdI_2 and LiI. The X-ray diffraction (XRD) data of the materials indicates that mainly single phase of tetrahedrite $Cu_{10}Cd_2Sb_4S_{13}$ compound is formed in both flux salts. XRD pattern of TH—Cd crystals grown in LiI reveals a shift of all diffraction peaks, lower CdS content and a smaller lattice parameter values in comparison with those formed in CdI_2. Energy dispersive X-ray spectroscopy reveals stoichiometric composition of $Cu_{10}Cd_2Sb_4S_{13}$ crystals grown in CdI_2 and Cu-poor grown in LiI. Analysis by Atomic Absorption Spectroscopy confirms the incorporation of Li into TH—Cd crystals at the level of 6.7×10^{20} at/cm^3. The photoluminescence (PL) study of $Cu_{10}Cd_2Sb_4S_{13}$ microcrystals at $T = 10$ K shows single broad asymmetric photoluminescence bands with the maxima at around 1.08 and 1.16 eV for materials grown respectively in CdI_2 and LiI. The thermal quenching activation energy of this PL band is $E_A = 88 \pm 6$ and 199 ± 7 meV for TH—Cd crystals grown in CdI_2 and LiI, respectively. Changes in the lattice parameters, composition and shift in PL maximum give evidences of Li incorporation from LiI into the crystal lattice of TH—Cd forming $Cu_{10-x}Li_xCd_2Sb_4S_{13}$ solid solution.

1. Introduction

Copper containing semiconductor compounds such as copper indium gallium sulfo-selenide [1], copper zinc tin sulfo-selenide [2] and sulfides containing copper and antimony (CAS) [3], can have a good prospect to be used as solar cell absorber materials due to the *p*-type conductivity originating from the copper deficient composition. From the CAS class sulfosalt compounds - $CuSbS_2$ (chalcostibite), $Cu_{12}Sb_4S_{13}$ (tetrahedrite, TH), Cu_3SbS_3 (skinnerite) and Cu_3SbS_4 (famatinite) - chalcostibite and tetrahedrite can have good prospective as solar absorbers [4]. TH compounds are widely studied as thermoelectric materials [5–7] and lately also as solar absorber materials due to their high absorption coefficient and *p*-type electrical conductivity [8]. These properties have encouraged significant scientific effort into synthesis of tetrahedrite semiconductor compounds for use in energy related applications using different methods.

Monograin powder (MGP) growth technology in molten salts as flux materials is one of the cheapest methods to synthesize multi-element semiconductor compounds [9–13]. The growth of powder crystals takes place at temperatures higher than the melting point of the used flux material and could be performed at temperatures much lower than the melting point of the formed target compound [10,14]. In the molten salt synthesis-growth process, the chemical nature of the liquid phase of the used flux salt controls the shape, size and the composition of the produced materials' crystals. The isothermal recrystallization of formed powder particles in molten fluxes is a suitable method to produce homogeneous single-crystalline grains. Several flux materials have been used for synthesis or recrystallization of MGPs. In [11,13], the formation of $Cu_2ZnSnSe_4$ in molten potassium, sodium and cadmium iodides was described. It was found by differential thermal analysis method that the intensive formation process of this quaternary compound starts close to the melting point of the used molten flux (KI or NaI) and results in homogeneous powders. In [15], polycrystalline SnS was recrystallized in different molten salts CdI_2, $SnCl_2$ and KI at different growth temperatures. Compositional analysis revealed single phase SnS MGPs at 740 °C in KI and at 500 °C in $SnCl_2$. However, the recrystallization of SnS in molten CdI_2 resulted in multiphase composition – beside SnS recrystallization, also CdS and Sn_2S_3 were formed. Furthermore, these

* Corresponding author.

https://doi.org/10.1016/j.tsf.2021.138980
Received 29 June 2021; Received in revised form 25 October 2021; Accepted 25 October 2021
Available online 29 October 2021

investigations proved that the morphology and composition of crystals can be controlled by the nature of the used flux materials.

In our previous studies [16,17], $Cu_{10}Cd_2Sb_4S_{13}$ (TH—Cd) MGPs were synthesized in the liquid phase of CdI_2 at 480 and 495 °C. It is known that monograins can form in the presence of liquid phase sufficient to avoid the sintering of primary crystals [10]. Therefore, the influence of volume ratio of liquid to solid phases (V_L/V_S) (volume of liquid CdI_2 to volume of solid $Cu_{12}Sb_4S_{13}$) to the composition and shape of TH—Cd MGP crystals was studied [12]. It was found that Cd from CdI_2 incorporated into $Cu_{12}Sb_4S_{13}$ crystals forming $Cu_{10}Cd_2Sb_4S_{13}$ whereby the incorporated Cd content increased with the increasing amount of added CdI_2. By applying the synthesis conditions where $V_L/V_S = 1$ was kept constant and CdS was used as the main Cd-source, mainly single-phase homogeneous TH—Cd material was finally gained. However, the powder contained some amount of sintered crystals and most of the crystals were smaller than 25 μm.

The produced monograin materials are subjected to be implemented as absorbers in monograin layer (MGL) solar cells. The MGL consists of a layer of unisize TH—Cd grains (for example the fraction size 45–56 μm) fixed by an organic resin (epoxy), more details about the MGL structure can be found in [14]. The present study deals with the formation of $Cu_{10}Cd_2Sb_4S_{13}$ MGPs in molten LiI and CdI_2. The influence of the two different fluxes to the properties of formed TH—Cd materials is compared. The molten media CdI_2 seems to be preferable due to its low hygroscopicity and low melting temperature (T_M = 387 °C [18]) that allows to reduce the synthesis temperature. Melting temperature of LiI is higher (T_M = 469 °C [18]) and LiI is very hygroscopic. The hygroscopic nature of LiI requires the preparation of synthesis samples only in a glove box in dry environment. The purpose of the present comparative study is to select proper growth conditions to produce homogeneous single phase $Cu_{10}Cd_2Sb_4S_{13}$ monograin powders usable for MGL solar cell applications.

2. Methodology

The $Cu_{10}Cd_2Sb_4S_{13}$ powder materials were synthesized from commercially available CdS (5 N) and self-synthesized Cu_2S (5 N) and Sb_2S_3 (5 N) by isothermal synthesis-growth method in two different molten fluxes, cadmium iodide (CdI_2) and lithium iodide (LiI). The volume ratio of solid precursors for TH—Cd to flux salt $V_{TH—Cd}/V_{flux}$ (cm^3/cm^3) = 1 was kept constant. The mixtures were heated in sealed vacuum quartz ampoules at 495 °C for 336 h. The grown powder particles were released from flux salt by leaching with deionized H_2O. After the removal of flux, the obtained powder crystals were dried in a hot-air thermostat at 50 °C and sieved into narrow size fractions by sieving system Retsch AS 200. More details about the monograin growth process of TH compound could be found elsewhere [16,17].

The sieved $Cu_{10}Cd_2Sb_4S_{13}$ MGP crystals with the size 56–63 μm were used as the absorber material in monograin layer solar cells with the following structure: graphite/$Cu_{10}Cd_2Sb_4S_{13}$/CdS/i-ZnO/ZnO:Al/Ag/glass. In the MGL solar cells every single $Cu_{10}Cd_2Sb_4S_{13}$ crystal covered with the CdS buffer layer, is working as an individual solar cell in parallel connection. The absorber layer (MGL membrane) was formed by embedding the TH—Cd grains halfway to a thin epoxy layer. After polymerization of epoxy, CdS buffer layer was deposited by the chemical bath deposition method. Subsequently, the membranes were covered with i-ZnO and conductive ZnO:Al layers by using the RF sputtering system. The silver paste was used to make the front collector onto the ZnO window layer and the front contact side of structure was glued onto a glass plate. The surfaces of the powder crystals at the back contact side were opened partly from epoxy by etching with concentrated H_2SO_4. After etching, the crystals` surfaces on the back contact side were activated by a mechanical abrasive treatment. A conductive graphite paste dots with an area of 0.052 cm^2 were used for making the back contacts.

The structure of the formed TH–Cd powder crystals was determined by X-ray diffraction (XRD) using a Rigaku Ultima IV diffractometer (Bragg-Brentano geometry) with monochromatic Cu Kα (Kα1, Kα2) radiation (λ = 1.5406 Å) at 40 kV and 40 mA operating with the silicon strip detector D/teX Ultra. PDXL 2 software was used for the derivation of crystal structure information from the powder XRD data (ICDD PDF-2–2019, 00–024–1317). The shape and surface morphology of the synthesized powder crystals were investigated by high-resolution scanning electron microscope (SEM), Zeiss Ultra 55. In-lens secondary electron detection at accelerating voltage of 4 kV was used. The chemical composition of the powder crystals was determined from polished cross-section of crystals` bulk by the energy dispersive X-ray spectroscopy (EDX) using a Bruker Esprit 1.82 system equipped with EDX-XFlash 3001 detector with an accelerating voltage of 20 kV (the measurement error is about 0.5 at.%). The phase composition of the powder crystals was studied by RT micro-Raman spectroscopy using Horiba's LabRam HR 800 spectrometer equipped with a multichannel CCD detector in the backscattering configuration. The 532 nm laser line with a spot size of about 5 μm was focused on the individual crystals (at least 6 in every case) of a powder. The bulk of crystals was studied from polished cross-section of samples. For the low-temperature (T = 10 K) photoluminescence (PL) measurements, a 0.64 m focal length single grating (600 mm^{-1}) monochromator and the 442 nm line of a He–Cd laser was used. PL signal was detected by a Hamamatsu InGaAs photomultiplier tube. The focused laser beam spot size was about 3 mm. The PL peak position measurement error is 0.005 eV. Current density versus voltage characteristics were recorded for the characterization of the MGL solar cells by a Keithley 2400 source metre under standard test conditions (AM 1.5, 100 mW/cm^2) using Newport Class AAA solar simulator system.

3. Results and discussions

3.1. XRD analysis

XRD patterns of $Cu_{10}Cd_2Sb_4S_{13}$ monograin powders synthesized in CdI_2 and LiI are presented in Fig. 1. XRD patterns of both materials show cubic crystal structure of tetrahedrite $Cu_{10}Cd_2Sb_4S_{13}$ phase with the space group I-43 m (ICDD PDF-2–2019, 00–024–1317) as a major phase with reflections of CdS as a minor secondary phase. These findings are in a good agreement with our previous studies [16,17] and literature [19]. XRD pattern of TH—Cd crystals grown in LiI (green line) reveals a shift of the diffraction peaks toward higher angles. The enlarged view of the

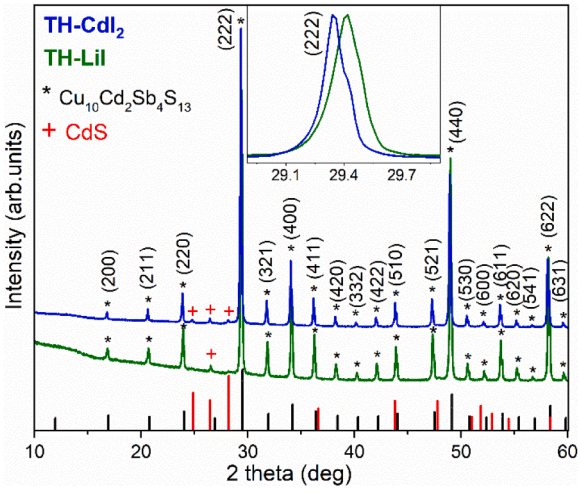

Fig. 1. X-ray diffraction patterns of the $Cu_{10}Cd_2Sb_4S_{13}$ MGPs grown in CdI_2 (blue line) and in LiI (green line). Inset graph presents the enlarged view of the shift of the (222) diffraction peak positions (ICDD PDF-2–2019, 00–024–1317). (For interpretation of the references to colour in this figure legend, the reader is referred to the web version of this article.)

shift of (222) lattice plane diffraction peak from 29.35 to 29.42 Å is presented in the inset graph in Fig. 1. Asymmetry of diffraction peaks in inset graph of Fig. 1 is caused by weak Kα2 X-ray contribution. The crystals grown in LiI have smaller lattice parameter in comparison with those formed in CdI_2 (LiI: $a = b = c = 10.509$ Å; CdI_2: $a = b = c = 10.512$ Å) indicating to a slight shrinkage of lattice. Similar lattice behaviour was recognized in kesterites where the incorporated Li^+ (ion radius 0.73 Å) was partly replacing Cu^+ ions (0.74 Å) in the crystal lattice of kesterites [20,21].

3.2. Morphology and particle size distribution

Monograin powder crystals growth are influenced by synthesis temperature, time, solubility and diffusion properties of used components in the selected flux material [14,22,23]. Therefore, morphology and particle size distribution of TH—Cd powders grown in molten CdI_2 and LiI were studied.

The morphology of TH—Cd crystals synthesized in CdI_2 and LiI can be seen in SEM images in Fig. 2. Most of the powder crystals grown in CdI_2 have flat surfaces and sharp edges, also sintered irregular agglomerates were detected. These observations indicate to an insufficient recrystallization of crystals and to some sintering process. Sintering is caused by the contracting capillary forces that arise in the solid–liquid phase boundaries due to insufficient amount of liquid phase [14]. The primary sintering of precursors' particles before the melting of flux salt can occur if some substance with melting temperatures lower than that of flux, exists in the initial mixture or it forms from components of precursors' mixture. Therefore, it must be considered that the sintered agglomerates found in the MGP grown in CdI_2 can refer to some chemical interaction of CdI_2 with precursor compounds producing a low melting product that conduce to the sintering. SbI_3 was detected at the walls of the synthesis ampoule by its ruby-red colour and Raman peak at 161 cm^{-1} [24]. As SbI_3 melts at 170.5 °C [18], it can act as sintering agent.

The primary sintering of solid particles can occur until the melting of CdI_2 at 387 °C. Once the liquid medium formed from molten flux salt is the dominant one, the solid particles repel from each other, and the crystallites formed in the synthesis reaction start to recrystallize and grow. The primary sintering can influence the shape and morphology of particles of the final product powder, also the size distribution.

TH—Cd MGPs grown in LiI resulted in well-formed individual crystals with rounded edges and smooth facets (see Fig. 2), probably due to a higher solubility of precursors and/or formed compound in LiI than in CdI_2.

The particle size distribution of powders was characterized by sieving analysis. The synthesized TH—Cd materials were sieved into narrow granulometric fractions between 38 μm to 250 μm. The sieving analysis results of the two materials show a considerable difference in the crystals' size distributions (see Fig. 3). Both materials have the Gaussian grain size distribution while the curve of TH—Cd grown in LiI (green bar chart) has the maximum in the range of bigger sizes (56–63 μm) than that of grown in CdI_2 (38–45 μm).

In closed ampoules in the isothermal conditions and in molten salt media, the formed solid particles of the product compound start to recrystallize and grow by the mechanism of Ostwald ripening [16] that predicts the Gaussian size distribution of product powder particles. The Ostwald ripening is a process [25] where the crystals grow due to the different surface energies of crystals of different sizes. The difference in surface energy (the reduction in total surface energy) is the only driving force of the transport of material from smaller to larger grains. The difference in the crystal's size means difference in the crystal's surface energy, thus smaller grains with higher surface energy dissolve in the used flux material and large grains grow after the materials' transport through molten phase by diffusion. The rate of diffusion is depending on viscosity of the transport media [26]. CdI_2 belongs to the group of 2B metal halides. By structural studies and first-principles calculations it is found that the melt of group 2B metal halides MX_2 (M=Zn, Cd, Hg and X=Cl, Br, I) have a structural model in which the small M_2^+ ions occupy tetrahedrally coordinated sites in a closely packed anion structure with strong intermediate range ordering [20–23]. The observed structure of melt leads to extremely low values of the ionic conductivity and to extremely high values of viscosity of the melt [27], viscosity of CdI_2 is 8.29 mPa × s at the growth temperature of 495 °C [26]. Vice versa, molten LiI has properties of a ionic liquid [28] and the viscosity at 495 °C is 1.91 mPa × s [29]. Therefore, the growth of crystals in CdI_2 is inhibited due to the lower transport rate of material.

3.3. Chemical composition

From the data of EDX analysis the chemical formulas of the synthesized powders were calculated taking into consideration the charge neutrality condition. The average chemical composition of the TH—Cd powder grown in CdI_2 is slightly Cu- and Sb-rich as can be seen from the formula $Cu_{10.1}Cd_{1.93}Sb_{4.07}S_{13}$. However, a Cu-poor composition with $Cu_{9.68}Cd_{1.96}Sb_{4.06}S_{13}$ was determined by EDX for crystals grown in LiI. In addition, EDX measurements revealed in the powders some separate crystals with chemical composition of Cd: $S = 49$: 50 at.%, indicating to the CdS as secondary phase. Less CdS crystals were detected if the TH—Cd was grown in LiI. Also, XRD results (see Fig. 1) correlate well with this last finding. The Cu index in TH—Cd crystals grown in LiI is decreased in comparison with that of TH—Cd grown in CdI_2. The decreased Cu content indicate to the possibility that Li from the used

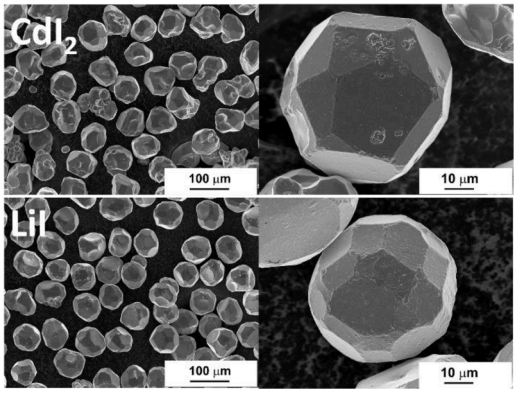

Fig. 2. SEM micrographs of $Cu_{10}Cd_2Sb_4S_{13}$ monograin powder crystals' grown in CdI_2 and in LiI.

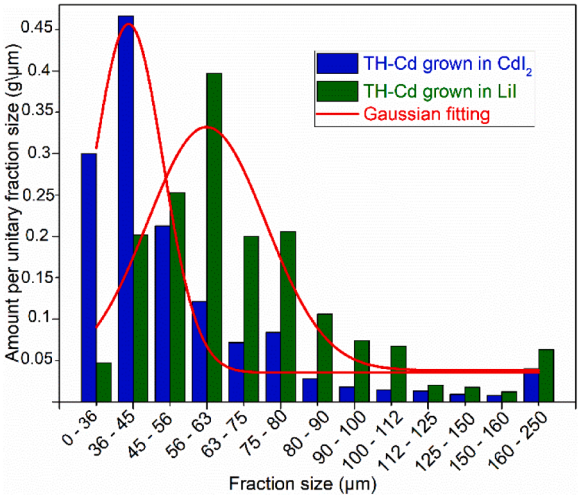

Fig. 3. Particle size distribution of $Cu_{10}Cd_2Sb_4S_{13}$ monograin powders grown in CdI_2 and LiI.

molten LiI incorporates into the $Cu_{10}Cd_2Sb_4S_{13}$ crystals lattice at the Cu site. In our previous study [16], the incorporation of Cd from the molten CdI_2 into $Cu_{12}Sb_4S_{13}$ was described.

Therefore, we believe that the incorporation of Li from the used molten LiI into the $Cu_{10}Cd_2Sb_4S_{13}$ crystals lattice could be possible. The atomic absorption spectroscopy (AAS) analysis of TH—Cd grown in LiI confirmed that Li content in TH—Cd crystals was 6.7×10^{20} at/cm^3. As Li^+ has ionic radius close to Cu^+ and taking into consideration that copper content in LiI grown TH—Cd was decreased, we propose a partial replacement of Cu^+ by Li^+. As a result, the incorporation of Li from the molten LiI into TH—Cd crystals, forming $Cu_{10-x}Li_xCd_2Sb_4S_{13}$ solid solution, is confirmed and the Cu-poor composition is explained.

To sum up, the above given findings provide insight into the growth mechanism of TH—Cd powder crystals in molten CdI_2 and LiI, and show that it is important to consider the nature of the liquid media where to obtain product crystals with the desired properties (morphology, crystals' size, the phase and chemical composition).

3.4. Raman spectroscopy analysis

In order to support the findings gained by XRD and EDX about $Cu_{10}Cd_2Sb_4S_{13}$ MGPs crystals grown in CdI_2 and in LiI, RT Raman analysis was used. Raman spectra are presented in Fig. 4. Lorentzian function was used for fitting to resolve all the Raman peaks. Fitted modes of the spectra of TH—Cd crystals grown in CdI_2 (96, 111, 130, 165, 247, 291, 327, 352 and 363 cm^{-1}) and in LiI (95, 111, 133, 175, 251, 291, 327, 354 and 363 cm^{-1}) are characteristic to the Cd substituted tetrahedrite. These Raman peaks are in good correlation with our previous works [16,17] and literature [3,30]. Raman spectra of the materials synthesized in two different molten salts reveal two main and intensive peaks at the same positions, at 111 cm and 363 cm^{-1}. In addition to those, some of the less intensive peaks are shifted if LiI was used: from 96 to 95 cm^{-1}, from 130 to 133 cm^{-1}, from 165 to 175 cm^{-1}, from 251 to 247 cm^{-1} and from 354 to 352 cm^{-1} (see Fig. 4). These shifts could be the confirmation of the incorporation of Li into the lattice of tetrahedrite and formation of $Cu_{10-x}Li_xCd_2Sb_4S_{13}$.

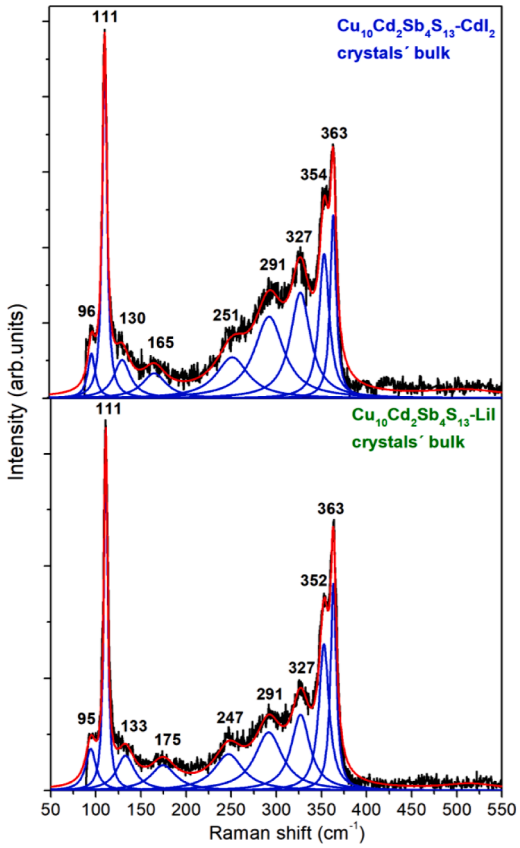

Fig. 4. Raman spectra recorded from polished samples of $Cu_{10}Cd_2Sb_4S_{13}$ crystals grown in CdI_2 and in LiI. Results of Lorentzian fittings are shown as solid blue lines. Laser excitation wavelength $\lambda = 532$ nm and power 0.42 mW were used. (For interpretation of the references to colour in this figure legend, the reader is referred to the web version of this article.)

3.5. Photoluminescence analysis

In order to study the recombination processes of $Cu_{10}Cd_2Sb_4S_{13}$ MGPs crystals grown in CdI_2 and in LiI, the photoluminescence measurements were conducted. Fig. 5 presents the low temperature (LT) ($T = 10$ K) PL spectra of TH—Cd crystals grown in CdI_2 (blue line) and in LiI (green line). Both PL spectra of $Cu_{10}Cd_2Sb_4S_{13}$ powder crystals at $T = 10$ K show a single broad, asymmetric PL bands with the maxima detected at around 1.08 and 1.16 eV for materials grown in CdI_2 and LiI, respectively. The PL spectrum of the material synthesized in LiI is shifted to the higher energy values.

In our previous study [17], the temperature and laser power dependencies for TH—Cd synthesized in CdI_2 were investigated. It was found that the PL band is related to donor-acceptor pair recombination where the activation energy of the acceptor defect was E_A=88±6 meV. The thermal activation energy for the PL band in LiI grown TH was obtained from the Arrhenius plot (Fig. 6) where the dependence of ln $\Phi(T)$ versus $1000/T$ was fitted by using theoretical expression for discrete energy levels [31]:

$$\Phi(T) = \Phi_0 / \left[1 + A_1 T^{3/2} + A_2 T^{3/2} \exp(-E_A / kT)\right] \quad (1)$$

where Φ is an integrated intensity of the PL band ($\Phi_0 = 0.009 \pm 0.004$), A_1 and A_2 are the process rate parameters ($A_1 = 0.0005 \pm 0.00006$; $A_2 = 30 \pm 11$) and E_A is the thermal activation energy.

Fitting results are also presented in Fig. 6. The thermal activation energy of PL band represents the depth of acceptor level E_A= 199±7 meV.

Temperature dependence of the peak position of PL band is depicted in Fig. 7. It is clearly visible that at LT the peak position of the PL-band shifts rapidly towards low energies linearly with temperature. This is a temperature region where the energy gap E_g has usually very slow temperature dependence. However, this quite rapid red-shift is typical for highly doped materials where the high concentration of intrinsic defects creates potential fluctuations and valence and conduction band tails. Moreover, these potential fluctuations affect also deep levels and as a result, PL bands will widen. According to [32,33] the E_{max} for PL-band

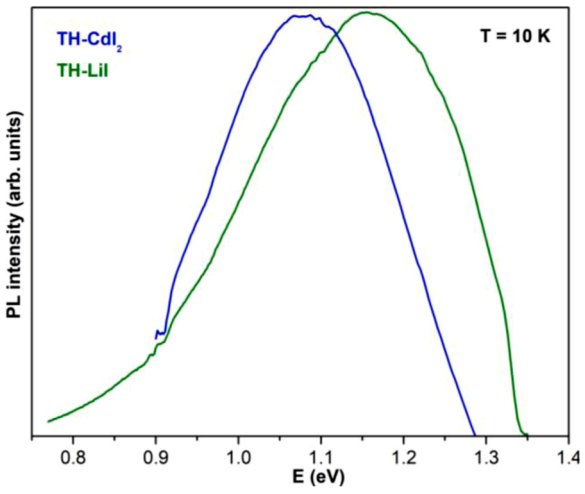

Fig. 5. Normalized PL spectra of $Cu_{10}Cd_2Sb_4S_{13}$ MGPs grown in CdI_2 and in LiI at $T = 10$ K.

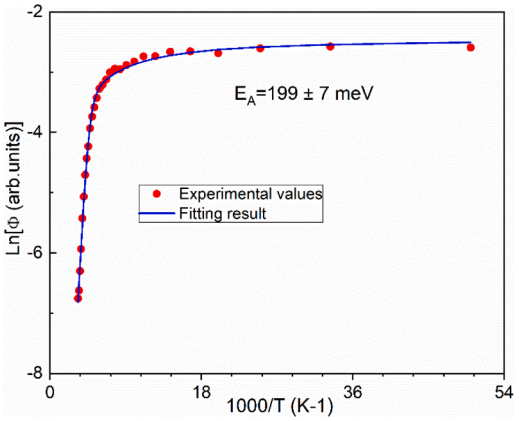

Fig. 6. Arrhenius plot of integral intensity Φ for PL band together with fitting result obtained using Eq. 1.

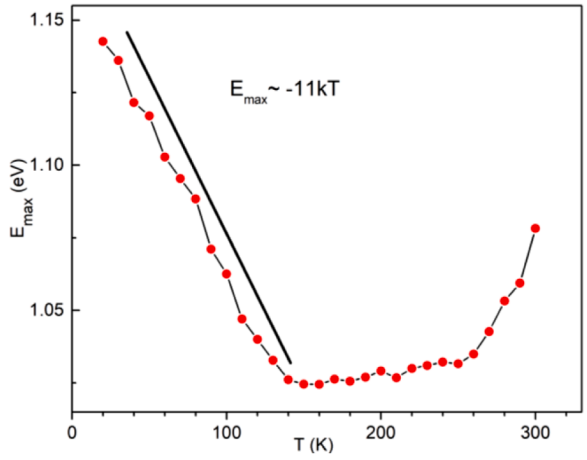

Fig. 7. Temperature dependence of PL band peak position of $Cu_{10}Cd_2Sb_4S_{13}$ crystals grown in LiI.

related to the recombination of free electrons with holes captured by deep acceptor levels in highly doped materials at low temperatures may be expressed as:

$$E_{max} \approx E^0_{max} - kTln[N_V / (p + n\Theta)] \quad (2)$$

where E^0_{max} is a peak position of the PL band at $T = 0$ K, N_V-is an effective density of states in the valence band, n, p- concentration of free electrons and holes, respectively, Θ-ratio of electron and hole capture probabilities by localized state. We neglected here the temperature dependence of E_g, because it has usually quite slow shift with temperature at low temperature region. In most highly doped materials the typical red-shift rate is around −4–7kT while in our samples it is about −11kT, see Fig. 7. According to Eq. (2) this is possible when the carrier concentration is very low and we have highly compensated material. In our previous paper [13] we showed that the PL band in CdI_2-grown TH—Cd had very different behaviour explained by the model of donor-acceptor pair recombination. We did not discover a presence of potential fluctuations in this material. The low hole concentration can be caused by the compositional peculiarity of formed $Cu_{10-x}Li_xCd_2Sb_4S_{13}$ solid solution. The actual mechanism of the compensation in TH—Cd grown in LiI is not known at the moment and further studies are needed. We can only assume that partly it could be related to incorporation of Li into copper vacancies V_{Cu}. It is known that V_{Cu} in these compounds is usually dominating shallow acceptor defect. However, high concentration of different donor-acceptor defect complexes can lead to high level of compensation.

By increasing the laser power, the shape of the PL spectra did not show any dramatic changes and the experimental data can be fitted by the simple power law of the form $\Phi \propto L^m$, where Φ is the PL integrated intensity, L is the excitation laser power and m is a dimensionless exponent. It is well known that for an excitation laser photon with an energy exceeding the band gap energy the coefficient m is generally $1 < m < 2$ for the free- and bound-exciton emission, and $m \leqq 1$ for free-to-bound and donor–acceptor pair recombinations [34]. We obtained the value of $m = 0.75 \pm 0.01$ for LiI grown TH PL band and this is a sign that the measured PL band is indeed related to deep defects.

3.6. MGL solar cell device properties

TH—Cd MGPs grown in CdI_2 and in LiI were used as absorber layers in MGL solar cells. The J–V curves of the devices measured in the dark and under illumination, are presented in Fig. 8. The best MGL solar cell based on $Cu_{10}Cd_2Sb_4S_{13}$ absorber grown in CdI_2, shows the open circuit voltage (V_{oc}) value of 377.32 mV, current density (J_{sc}) of 0.94 mA/cm^2, fill factor (*FF*) of 51.3% and power conversion efficiency (PCE) of 0.18% while the MGL solar cell based on TH—Cd MGP grown in LiI has V_{oc} value of 505.8 mV, J_{sc} of 4.46 mA/cm^2 and *FF* of 50%, resulting in PCE of 1.13%. So far, this is the highest achieved power conversion efficiency of tetrahedrite solar cell. These results show that both $Cu_{10}Cd_2Sb_4S_{13}$ MGPs grown in CdI_2 and in LiI are potential candidates as absorber materials in photovoltaic devices. MGL solar cells based on TH—Cd grown in LiI have better performance than these ones grown in CdI_2, most probably due to the decreased Cu content in the MGP crystals. Therefore, the investigations based on the dependence of optoelectronic parameters on compositional properties are a subject for further studies.

4. Conclusion

In this study, it is shown that the synthesis-growth of $Cu_{10}Cd_2Sb_4S_{13}$ MGP crystals is possible in both used molten fluxes, in CdI_2 and LiI. XRD pattern of TH—Cd crystals grown in

LiI revealed a shift of the reflexions, a smaller lattice parameter values and a lower CdS content in comparison with those formed in CdI_2 ($Cu_{10}Cd_2Sb_4S_{13}$ synthesized in LiI: $a = b = c = 10.509$ Å and in CdI_2: $a = b = c = 10.512$ Å). Based on EDX analysis, the TH—Cd powder crystals grown in CdI_2 had a chemical composition close to the stoichiometry. The synthesis-growth of TH—Cd in LiI resulted in Cu-poor composition but with a Li content at the level of 6.7×10^{20} at/cm^3, as determined by AAS analysis. The synthesis-growth in CdI_2 caused remarkable amount of sintered grains, while uniform individual crystals with rounded edges

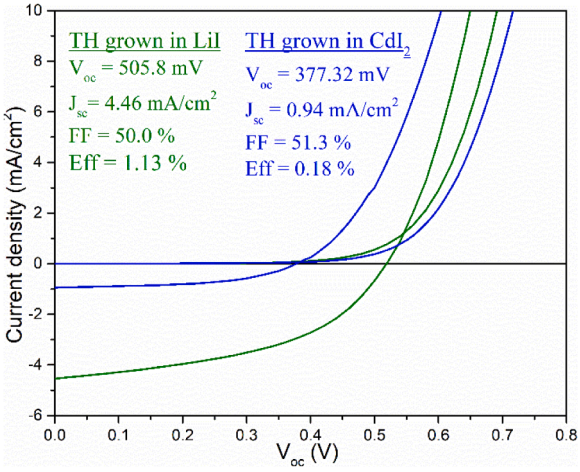

Fig. 8. Current-voltage characteristics of MGL solar cell based on $Cu_{10}Cd_2Sb_4S_{13}$ grown in CdI_2 and in LiI.

and smooth facets were formed in LiI, as detected by SEM. The granulometric analysis showed the Gaussian size distribution of particles for both materials, characteristic to the growth mechanism of "Ostwald ripening", that allows to conclude that the latter mechanism is prevailing in the crystal's growth. The maxima of size distribution curves are at different sizes – bigger crystals were gained in LiI. The faster growth rate in LiI was attributed to the lower viscosity of molten LiI enabling faster diffusion of material from grain to grain.

Low-temperature (T = 10 K) photoluminescence spectra of $Cu_{10}Cd_2Sb_4S_{13}$ crystals grown in CdI_2 and LiI were dominated by broad and asymmetric PL bands with maxima at 1.08 and 1.16 eV, respectively. The thermal quenching activation energies of PL bands were E_A= 88±6 and 199±7 meV for these materials grown in CdI_2 and LiI, respectively. It was found that the TH—Cd grown in LiI was highly compensated. The actual mechanism of compensation is not known at the moment and further studies are needed.

Based on the results of this study, it was concluded that Li^+ from the molten flux (LiI) incorporated into the $Cu_{10}Cd_2Sb_4S_{13}$ crystals structure and most probably, by replacing part of Cu^+ sites in the lattice formed $Cu_{10-x}Li_xCd_2Sb_4S_{13}$ solid solution. The $Cu_{10}Cd_2Sb_4S_{13}$ MGL solar cell based on absorber material grown in LiI performed the efficiency of 1.13% (V_{oc} = 505.8 mV, J_{sc} = 4.46 mA/cm^2 and FF = 50%). The achieved power conversion efficiency is a record for tetrahedrite based photovoltaic devices.

Declaration of Competing Interest

The authors declare that they have no known competing financial interests or personal relationships that could have appeared to influence the work reported in this paper.

Acknowledgements

This work was supported by the Estonian Ministry of Education and Research, Estonian Research Council project PRG1023, by ERDF project center of nanomaterials technologies and research (NAMUR+)" (2014–2020.4.01.16–0123) and by the European Union through the European Regional Development Fund, Project TK141 and Dora Plus Scholarship. M. Grossberg is thankful to the L'Oréal Baltic For Women in Science Program.

References

[1] M. Bouttemy, P. Tran-Van, I. Gerard, T. Hildebrandt, A. Causier, J.L. Pelouard, G. Dagher, Z. Jehl, N. Naghavi, G. Voorwinden, B. Dimmler, M. Powalla, J. F. Guillemoles, D. Lincot, A. Etcheberry, Thinning of CIGS solar cells: part I: chemical processing in acidic bromine solutions, Thin Solid Films 519 (2011) 7207–7211, https://doi.org/10.1016/j.tsf.2010.12.219.

[2] I. Leinemann, G.C. Nkwusi, K. Timmo, O. Volobujeva, M. Danilson, J. Raudoja, T. Kaljuvee, R. Traksmaa, M. Altosaar, D. Meissner, Reaction pathway to $Cu_2ZnSnSe_4$ formation in CdI_2, J. Therm. Anal. Calorim. 134 (2018) 409–421, https://doi.org/10.1007/s10973-018-7102-5.

[3] D.S. Prem Kumar, M. Ren, T. Osipowicz, R.C. Mallik, P. Malar, Tetrahedrite ($Cu_{12}Sb_4S_{13}$) thin films for photovoltaic and thermoelectric applications, Sol. Energy. 174 (2018) 422–430, https://doi.org/10.1016/j.solener.2018.08.080.

[4] K. Ramasamy, H. Sims, W.H. Butler, A. Gupta, Selective Nanocrystal Synthesis and Calculated Electronic Structure of All Four Phases of Copper–Antimony–Sulfide, Chem. Mater. 26 (2014) 2891–2899, https://doi.org/10.1021/cm5005642.

[5] A.V. Powell, Recent developments in Earth-abundant copper-sulfide thermoelectric materials, J. Appl. Phys. 126 (2019), 100901, https://doi.org/10.1063/1.5119345.

[6] O. Caballero-Calero, J.R. Ares, M. Martín-González, Environmentally Friendly Thermoelectric Materials: high Performance from Inorganic Components with Low Toxicity and Abundance in the Earth, Adv. Sustainable Syst. 112 (2021), 2100095, https://doi.org/10.1002/adsu.202100095.

[7] R. Chetty, A. Bali, R.C. Mallik, Tetrahedrites as thermoelectric materials: an overview, J. Mater. Chem. C. 3 (2015) 12364, https://doi.org/10.1039/C5TC02537K.

[8] J. Heo, R. Ravichandran, C.F. Reidy, J. Tate, J.F. Wager, D.A. Keszler, Design Meets Nature: tetrahedrite Solar Absorbers, Adv. Energy Mater. 5 (2015), 1401506, https://doi.org/10.1002/aenm.201401506.

[9] E. Mellikov, M. Altosaar, M. Kauk-Kuusik, K. Timmo, D. Meissner, M. Grossberg, J. Krustok, O. Volobujeva, Growth of CZTS-Based Monograins and Their Application to Membrane Solar Cells, in: K. Ito (Ed.), Copper Zinc Tin Sulfide-Based Thin Film Solar Cells, John Wiley & Sons Ltd, UK, 2015, pp. 289–309, https://doi.org/10.1002/9781118437865.ch13.

[10] E. Mellikov, J. Hiie, M. Altosaar, Powder materials and technologies for solar cells, Int. J. Mater. Prod. Technol. 28 (2007) 291, https://doi.org/10.1504/IJMPT.2007.013082.

[11] I. Leinemann, K. Timmo, M. Grossberg, T. Kaljuvee, K. Tõnsuaadu, R. Traksmaa, M. Altosaar, D. Meissner, Reaction enthalpies of $Cu_2ZnSnSe_4$ synthesis in KI, J. Therm. Anal. Calorim. 119 (2015) 1555–1564, https://doi.org/10.1007/s10973-018-7415-4.

[12] I. Leinemann, W. Zhang, T. Kaljuvee, K. Tõnsuaadu, R. Traksmaa, J. Raudoja, M. Grossberg, M. Altosaar, D. Meissner, $Cu_2ZnSnSe_4$ formation and reaction enthalpies in molten NaI starting from binary chalcogenides, J. Therm. Anal. Calorim. 118 (2014) 1313–1321, https://doi.org/10.1007/s10973-014-4102-y.

[13] I. Leinemann, M. Pilvet, T. Kaljuvee, R. Traksmaa, M. Altosaar, Reaction pathway to CZTSe formation in CdI_2, J. Therm. Anal. Calorim. 134 (2018) 433–441, https://doi.org/10.1007/s10973-018-7415-4.

[14] E. Mellikov, D. Meissner, T. Varema, M. Altosaar, M. Kauk, O. Volobujeva, J. Raudoja, K. Timmo, M. Danilson, Monograin materials for solar cells, Solar Energ. Mater. & Solar Cells. 93 (2009) 65–68, https://doi.org/10.1016/j.solmat.2008.04.018.

[15] K. Timmo, M. Kauk-Kuusik, M. Pilvet, V. Mikli, E. Kärber, T. Raadik, I. Leinemann, M. Altosaar, J. Raudoja, Comparative study of SnS recrystallization in molten CdI_2, $SnCl_2$ and KI, Phys. Status Solidi C. 13 (2016) 8–12, https://doi.org/10.1002/pssc.201510082.

[16] F. Ghisani, K. Timmo, M. Altosaar, J. Raudoja, V. Mikli, M. Pilvet, M. Kauk-Kuusik, M. Grossberg, Synthesis and characterization of tetrahedrite $Cu_{10}Cd_2Sb_4S_{13}$ monograin material for photovoltaic application, Mater. Sci. Semicond. Process. 110 (2020), 104973, https://doi.org/10.1016/j.mssp.2020.104973.

[17] J. Krustok, T. Raadik, R. Kaupmees, F. Ghisani, K. Timmo, M. Altosaar, V. Mikli, M. Grossberg, Broad-band photoluminescence of donor-acceptor pairs in tetrahedrite $Cu_{10}Cd_2Sb_4S_{13}$ microcrystals, J. Phys. D: Appl. Phys. 54 (2021), 105102, https://doi.org/10.1088/1361-6463/abce29.

[18] D.R. Lide, H.P.R. Frederikse, CRC Handbook of Chemistry and Physics, 78th ed., CRC Press, Boca Raton FL, New York, (1997-1998).

[19] D.S. Prem Kumar, R. Chetty, P. Rogl, G. Rogl, E. Bauer, P. Malar, R.C. Mallik, Thermoelectric properties of Cd doped tetrahedrite: $cu_{12-x}Cd_xSb_4S_{13}$, Intermetallics 78 (2016) 21–29, https://doi.org/10.1016/j.intermet.2016.08.003.

[20] Y.E. Romanyuk, S.G. Haass, S. Giraldo, M. Placidi, D. Tiwari, D.J. Fermin, X. Hao, H. Xin, T. Schnabel, M. Kauk-Kuusik, P. Pistor, S. Lie, L.H. Wong, Doping and alloying of kesterites, J. Phys. Energy. 1 (2019), 044004, https://doi.org/10.1088/2515-7655/ab23bc.

[21] A. Lafond, C. Guillot-Deudon, J. Vidal, M. Paris, C. La, S. Jobic, Substitution of Li for Cu in Cu_2ZnSnS_4: toward Wide Band Gap Absorbers with Low Cation Disorder for Thin Film Solar Cells, Inorg. Chem. 56 (2017) 2712–2721, https://doi.org/10.1021/acs.inorgchem.6b02865.

[22] M. Altosaar, E. Mellikov, $CuInSe_2$ Monograin Growth in CuSe-Se Liquid Phase, Jpn. J. Appl. Phys. 39 (2000) 65, https://doi.org/10.7567/jjaps.39s1.65.

[23] K. Timmo, M. Altosaar, M. Kauk, J. Raudoja, E. Mellikov, $CuInSe_2$ monograin growth in the liquid phase of potassium iodide, Thin Solid Films 515 (2007) 5884–5886, https://doi.org/10.1016/j.tsf.2006.12.085.

[24] A. Saitoh, T. Komatsu, T. Karasawa, H. Ohtake, T. Suemoto, Raman scattering under hydrostatic pressures in layered BiI_3 and SbI_3 crystals, Phys. Status Solidi Basic Res. 226 (2001) 357–367, https://doi.org/10.1002/1521-3951(200108)226:2<357::AID--PSSB357>3.0.CO;2-8.

[25] T. Bergfors, Seeds to crystals, J. Struct. Biol. 142 (2003) 66–76, https://doi.org/10.1016/S1047-8477(03)00039-X.

[26] K.A. Tasidou, Ch.D. Chliatzou, M.J. Assael, K.D. Antoniadis, S.K. Mylona, M. L. Huber, W.A. Wakeham, Reference Correlations for the Viscosity of 13 Inorganic Molten Salts, J. Phys. Chem. Ref. Data. 48 (2019), 013101, https://doi.org/10.1063/1.5091511.

[27] R. Triolo, A.H. Narten, X-ray diffraction study of molten zinc chloride at 323 °C, J. Chem. Phys. 74 (1980) 703–704, https://doi.org/10.1063/1.440829.

[28] G.E. Blomgren, E.R. Van Artsdalen, F.U.S.E.D. SALTS, Annual Rev. of Phys. Chem. 11 (1960) 273–306, https://doi.org/10.1146/annurev.pc.11.100160.001421.

[29] Y. Sato, M. Fukasawa, T. Yamamura, Viscosities of molten alkali-metal bromides and iodides, Int. J. Thermophys. 18 (1997) 1123–1142, https://doi.org/10.1007/BF02575253.

[30] S. Kharbish, E. Libowitzky, A. Beran, The effect of As-Sb substitution in the Raman spectra of tetrahedrite-tennantite and pyrargyrite-proustite solid solutions, Eur. J. Mineral. 19 (2007) 567–574, https://doi.org/10.1127/0935-1221/2007/0019-1737.

[31] J. Krustok, H. Collan, K. Hjelt, Does the low-temperature Arrhenius plot of the photoluminescence intensity in CdTe point towards an erroneous activation energy? J. Appl. Phys. 81 (1997) 1442–1445, https://doi.org/10.1063/1.363903.

[32] A.P. Levanyuk, V.V. Osipov, Edge luminescence of direct-gap semiconductors, Usp. Fiz. Nauk. 133 (1981) 427–477, https://doi.org/10.3367/UFNr.0133.198103b.0427.

[33] J. Krustok, H. Collan, M. Yakushev, K. Hjelt, The Role of Spatial Potential Fluctuations in the Shape of the PL Bands of Multinary Semiconductor Compounds, Phys. Scr. T79 (1999) 179, https://doi.org/10.1238/physica.topical.079a00179.

[34] T. Schmidt, K. Lischka, W. Zulehner, Excitation-power dependence of the near-band-edge photoluminescence of semiconductors, Phys. Rev. B. 45 (1992) 8989–8994, https://doi.org/10.1103/PhysRevB.45.8989.